PHYSICAL REVIEW A **94**, 050701(R) (2016)

Quantum-state-controlled Penning-ionization reactions between ultracold alkali-metal and metastable helium atoms

A. S. Flores, W. Vassen, and S. Knoop
LaserLaB, Department of Physics and Astronomy, Vrije Universiteit, De Boelelaan 1081, 1081 HV Amsterdam, The Netherlands
(Received 2 September 2016; published 3 November 2016)

In an ultracold, optically trapped mixture of ^{87}Rb and metastable triplet ^{4}He atoms we have studied trap loss for different spin-state combinations, for which interspecies Penning ionization is the main two-body loss process. We observe long trapping lifetimes for the purely quartet spin-state combination, indicating strong suppression of Penning-ionization loss by at least two orders of magnitude. For the other spin mixtures we observe short lifetimes that depend linearly on the doublet character of the entrance channel. We compare the extracted loss rate coefficient with recent predictions of multichannel quantum-defect theory for reactive collisions involving a strong exothermic loss channel and find near-universal loss for doublet scattering. Our work demonstrates control of Penning-ionization reactive collisions by internal atomic state preparation.

DOI: 10.1103/PhysRevA.94.050701

Ultracold inelastic and reactive collisions are important processes in atomic and molecular samples [1,2], determining their trapping lifetimes and the success of evaporative and sympathetic cooling. Conversely, measurements of these lifetimes reveal the rate coefficients of the dominant inelastic or reactive collision processes, opening the fields of ultracold few-body physics [3,4] and ultracold chemistry [5,6]. The ultracold regime offers exquisite control over the initial internal and external quantum states, and the possibility to experimentally control collision properties or even steer chemical reactions with external fields [7].

Understanding of inelastic and reactive collisions is in general very difficult due to the many degrees of freedom involved. This has motivated recent work based on multichannel quantum-defect theory (MQDT) [8–10], in which analytic expressions of collision rates were derived in the case of a strong exothermic reactive channel. In particular, if the probability of an inelastic or reactive process in the short-range part of the collision is 100%, i.e., if $P^{\mathrm{re}} = 1$, theory predicts universal rate constants that only depend on the reduced mass of the collision partners and the leading long-range coefficient [8,9], independent of the complicated short-range dynamics. If the reaction probability is less than 100% ($P^{\mathrm{re}} < 1$), still only two parameters are required to include the (nonuniversal) short-range physics, i.e., the scattering length a and P^{re} [10]. These analytical models have been applied to atom-exchange reactions between ground state KRb molecules below 1 μK [5,8], and Penning-ionization reactions between argon and helium atoms in the metastable triplet $2\,^3S_1$ state (He*) in merged-beam experiments from 10 mK up to 30 K [10,11].

In this Rapid Communication we study ultracold Penning-ionizing collisions between He* atoms (internal energy 19.8 eV) and alkali-metal atoms A in their electronic ground state:

$$\mathrm{He}(2\,^3S_1) + A(^2S_{1/2}) \rightarrow \mathrm{He}(1\,^1S_0) + A^+(^1S_0) + e^-, \qquad (1)$$

which are described by two interaction potentials, doublet $^2\Sigma^+$ and quartet $^4\Sigma^+$, and a strongly exothermic Penning-ionization (PI) reaction channel (see Fig. 1 for the specific case of He* + Rb). The description of the PI loss rate in terms of MQDT would require at least four parameters, namely, the scattering lengths and the reaction probabilities of both doublet and quartet potentials. However, PI from the $^4\Sigma^+$ potential is spin forbidden, because the total electron spin in the PI channel is only 1/2 [see Eq. (1)]. Thus PI proceeds predominantly via the doublet $^2\Sigma^+$ potential. Therefore one expects the PI loss rate to be determined by the $^2\Sigma^+$ potential only, however, including an additional factor that takes into account the doublet character of the particular entrance channel. This makes the PI loss rate experimentally controllable by internal atomic state preparation and magnetic field.

We have realized an ultracold mixture of ^{4}He* and ^{87}Rb in an optical dipole trap (ODT), and performed lifetime measurements for different spin-state combinations [the labeling of the atomic spin states is shown in Fig. 2: (*a*–*h*) for ^{87}Rb and (*A*–*C*) for ^{4}He*]. ODTs provide spin-independent confinement, applicable to both low- and high-field seeking spin states, which allows direct comparison between trap losses of different spin mixtures. Previous experimental studies of He*+alkali collisions have been performed at thermal energies in stationary afterglow and merged-beam experiments (see, e.g., [12,15]). Simultaneous laser cooling and trapping of ^{4}He* and ^{87}Rb was first demonstrated by the Truscott group [16]. Magnetic trapping of the $h + C$ spin-state combination, which is purely quartet, provided upper limits of the PI rate on the order of 10^{-12} cm^3 s^{-1} for pure quartet scattering [13,17], and revealed a small quartet scattering length a_Q [13], in agreement with *ab initio* calculations of the quartet $^4\Sigma^+$ potential [13,18]. In contrast, knowledge on the doublet $^2\Sigma^+$ potential is limited [12], and the doublet scattering length a_D is unknown.

The starting point of our measurements is an ultracold mixture of 3×10^4 ^{4}He* and 9×10^4 ^{87}Rb atoms in a single-beam ODT at a temperature of 22 and 15 μK, respectively. The main parts of our experimental setup are described earlier: dual-species magneto-optical trap and transfer to quadrupole magnetic trap (QMT) [13] and production of ^{87}Rb [19] and ^{4}He* [20] Bose-Einstein condensates using a single-beam ODT. Here we apply simultaneous radiofrequency (rf) and microwave (μw) forced evaporative cooling in the QMT for He* and Rb, respectively, before transfer to the single-beam ODT, which has a waist of 40 μm and a wavelength of 1557 nm. We use a fixed ODT power of 3.8 W, corresponding to an

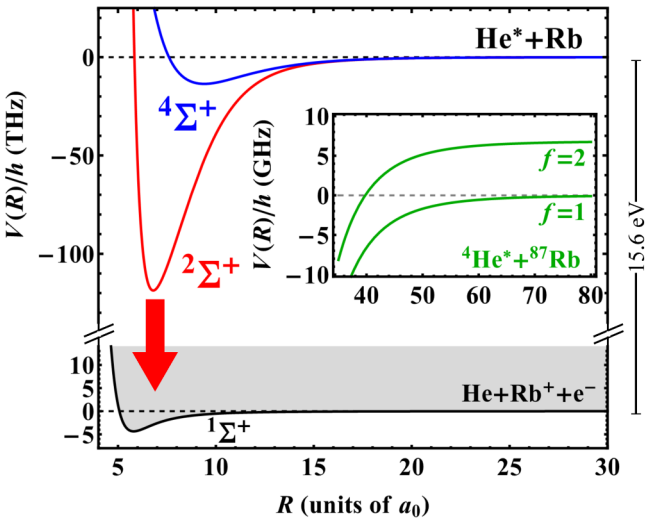

FIG. 1. Potential energy curves of the $^2\Sigma^+$ [12] and $^4\Sigma^+$ [13] states of the He*Rb molecule that correlate with the He*+Rb atomic asymptote, and the $^1\Sigma^+$ [14] state of the $HeRb^+$ molecule that correlates with the $He+Rb^+ + e^-$ asymptote, which lies 15.6 eV lower and forms the Penning-ionization continuum (where the internuclear distance R is given in Bohr radii, $a_0 = 0.052\,92$ nm). The inset shows the long-range adiabatic potentials of ^{4}He* ^{87}Rb near its dissociation threshold, including the hyperfine splitting of ^{87}Rb.

effective trap depth of 200 μK and 140 μK for He* and Rb, respectively [21].

Throughout the preparation stages in the QMT and ODT we use the stable $h + C$ spin-state combination [13]. To prepare other spin mixtures we transfer ^{87}Rb from h to a and/or ^{4}He* from C to A, by single adiabatic μw and rf frequency sweeps, respectively, at a bias magnetic field of 2.5 G. While our rf transfer has a 100% efficiency, our μw transfer is only 50% due to limited μw power. We remove the nontransferred Rb atoms in state h with resonant light immediately after the μw sweep. After a variable hold time we switch off the ODT and simultaneously measure the number of atoms by using standard absorption imaging for Rb and microchannel plate (MCP) detection for He* [22].

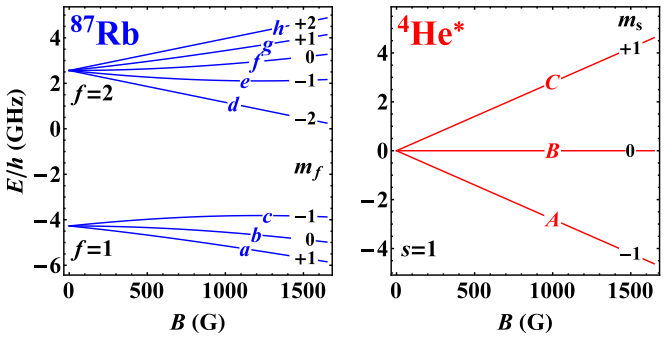

FIG. 2. Magnetic field dependence of the atomic ground-state energies of ^{87}Rb and ^{4}He*, indicating the labeling of the different internal states as used throughout the Rapid Communication.

We obtain the interspecies Penning-ionization loss rate coefficients by measuring the time evolution of the number of He* atoms, and fit the solution of two coupled equations:

$$\dot{N}_i = -\Gamma_i N_i - L_2 \int n_i(\vec{r}) n_j(\vec{r}) d\vec{r}, \tag{2}$$

where (i, j) is (He*, Rb), L_2 is the total interspecies two-body loss rate coefficient, and N_i and $n_i(\vec{r})$ are the atom number and density profile for species i. Intraspecies two- and three-body loss processes [23–25] can be fully neglected for the chosen spin states under our conditions. We only fit the time evolution of He*, using the measured initial Rb atom number, because of the higher sensitivity being the minority species and the better signal to noise of the He* MCP detection compared to the absorption imaging of Rb. The density profiles are calculated numerically, using measured temperatures T_i, via $n_i(\vec{r}) = n_i^0 \exp[-U_i(\vec{r})/k_B T_i]$, where $U_i(\vec{r})$ is the trapping potential, including gravity, and $n_i^0 = N_i / \int \exp[-U_i(\vec{r})/k_B T_i] d\vec{r}$ is the peak density. In our case the vertical confinement is strong enough such that the reduction of the overlap between the two clouds due to the differential gravitational sag is negligible. Single-species lifetimes are measured to determine the one-body loss rates Γ_i.

In Fig. 3 we present our lifetime measurements (at the bias magnetic field of 2.5 G), showing the time evolution of the He* atom number of the different spin mixtures. We observe a long trapping lifetime for the purely quartet $h + C$ spin combination, which we cannot distinguish from the single-species lifetimes. This means that the trapping lifetime is fully dominated by one-body loss and we can only obtain an upper limit of the two-body loss rate, namely, 1.3×10^{-12} cm^3 s^{-1}. Together with our knowledge of a_Q [13], we obtain a constraint on the reaction probability for the quartet $^4\Sigma^+$ potential of $P^{\mathrm{re}} < 0.01$, using Eq. (5) below. We expect the actual quartet PI loss rate to be on the order of 10^{-14} cm^3 s^{-1}, on the basis of the suppression of PI in homonuclear He* collisions [22] and the similar s character of the valence electron of He* and

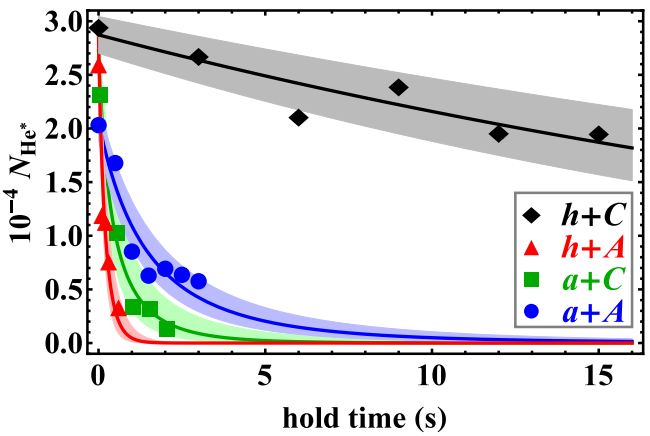

FIG. 3. Time evolution of the number of He* atoms for different spin mixtures, at a bias magnetic field of 2.5 G. The displayed data represent an average over several experimental runs (3–6). The solid lines are fits of Eq. (2) to all the data. The colored bands around the lines indicate the standard error of the fit. The initial Rb atom numbers are $h + A$ and $h + C$: $N_{\mathrm{Rb}} = (8.6 \pm 0.7) \times 10^4$; $a + A$: $N_{\mathrm{Rb}} = (4.5 \pm 0.8) \times 10^4$; $a + C$: $N_{\mathrm{Rb}} = (3.9 \pm 0.6) \times 10^4$.

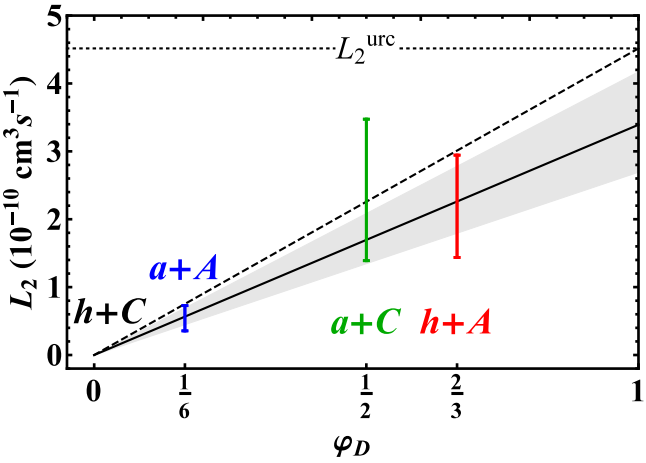

FIG. 4. Compilation of measured two-body loss rates L_2, sorted by the corresponding doublet character φ_D, and comparison with the universal loss rate L_2^{urc} (dotted line) via $L_2 = \varphi_D L_2^{\mathrm{urc}}$ (dashed line). The solid line is a linear fit through the data points (and its colored band indicates the standard error of the fit).

alkali-metal atoms. In the following we simply neglect the quartet contribution to the PI loss.

For the $h + A$, $a + C$, and $a + A$ spin mixtures we observe orders of magnitude faster losses, and especially for the $h + A$ and $a + C$ spin mixtures the He* sample is depleted within a few seconds. Here one should note the approximately factor of 2 difference in initial Rb atom numbers between the $h + A$ mixture and the $a + A$ and $a + C$ mixtures, mainly due to the μw transfer efficiency. We obtain the two-body loss rate coefficients L_2 by fitting Eq. (2) to the data, and the results are shown in Fig. 4. The error bars contain the fit error and uncertainty in the initial Rb atom number, as well as the uncertainty in the temperatures, which are required to calculate the density profile.

First we analyze our data in terms of the doublet character φ_D, which represents the amount of doublet scattering. Provided that PI is the dominant loss process, we expect the loss rate to scale linearly with φ_D,

$$L_2 = \varphi_D L_2^{\mathrm{PI}}, \tag{3}$$

where L_2^{PI} is the loss rate due to PI for pure doublet scattering. φ_D is obtained by expanding the long-range atomic product states on to the short-range doublet molecular state (see Supplemental Material [26]). In the limit of low magnetic fields, i.e., $B \ll E_{\mathrm{HFS}}/4\mu_B$ (where E_{HFS} is the alkali hyperfine splitting and μ_B is the Bohr magneton), and the case of an alkali-metal atom with nuclear spin of 3/2, φ_D takes values of $q/6$, where q is an integer number between 0 and 4. The value of φ_D for the different spin-state combinations is indicated in Fig. 4. Fitting Eq. (3) to our data gives $L_2^{\mathrm{PI}} = 3.4^{+0.8}_{-0.7} \times 10^{-10}\ \mathrm{cm}^3\ \mathrm{s}^{-1}$ for Penning-ionization loss via the doublet potential.

Second, we compare the obtained value of L_2^{PI} with analytic expressions from MQDT. For the universal case, $P^{\mathrm{re}} = 1$, the zero-temperature limit universal loss rate is given by [8,9]

$$L_2^{\mathrm{urc}} = 2\frac{h}{\mu}\bar{a}, \tag{4}$$

where $\bar{a} = 0.478\ldots(2\mu C_6/\hbar^2)^{1/4}$ is the so-called mean scattering length that solely depends on the reduced mass μ and the leading long-range van der Waals coefficient C_6. For He*+Rb, $C_6 = 3858$ a.u. [13], resulting for ^{4}He* +^{87}Rb in $\bar{a} = 41a_0$ and $L_2^{\mathrm{urc}} = 4.5 \times 10^{-10}\ \mathrm{cm}^3\ \mathrm{s}^{-1}$. In Fig. 4 L_2^{urc} and $\varphi_D L_2^{\mathrm{urc}}$ are shown as the dotted and dashed lines, respectively. Our extracted value of L_2^{PI} lies slightly below L_2^{urc}. However, taking into account a small finite temperature correction of 8% reduces the universal loss rate to $4.2 \times 10^{-10}\ \mathrm{cm}^3\ \mathrm{s}^{-1}$ (see Supplemental Material [26]), which is consistent with our L_2^{PI} and the reaction probability for PI in the doublet potential might be 100%.

Still, L_2^{PI} could also correspond to the nonuniversal case, $P^{\mathrm{re}} < 1$, where the zero-temperature limit loss rate is given by [10]

$$L_2^{\mathrm{nurc}} = L_2^{\mathrm{urc}} y \frac{1 + (s-1)^2}{1 + y^2(s-1)^2}, \tag{5}$$

where y is related to P^{re} via $P^{\mathrm{re}} = 4y/(1+y)^2$, and $s = a/\bar{a}$ is the rescaled scattering length, where a is the scattering length (here the doublet scattering length a_D). The combinations of P^{re} and s that match L_2^{PI} are shown in Fig. 5 as the purple band (for which we have also included finite temperature corrections). A typical scattering length of $a \approx \bar{a}$, i.e., $s \approx 1$, would mean a high reaction probability of $P^{\mathrm{re}} \gtrsim 0.94$. While for $P^{\mathrm{re}} = 1$ sensitivity to the scattering length is lost (and $L_2^{\mathrm{nurc}} = L_2^{\mathrm{urc}}$), a tiny reduction of less than 0.001 already results in a constraint on the possible scattering length range of about $0 \lesssim s \lesssim 2$. A match with a small reaction probability would require the less likely cases of either a large positive or large negative scattering length.

In principle, P^{re} can be calculated from the complex potential $U(r) = V(r) - (i/2)\Gamma(r)$ [27], where $\Gamma(r)$ represents the ionization width. For He*+alkali collisions, *ab initio* calculations on the doublet potential $V(r)$ and corresponding $\Gamma(r)$ are available for Li, Na, and K [28], from which one can estimate $P^{\mathrm{re}} \approx 0.6$–$0.7$. For He*+Rb, information on the doublet potential $V(r)$ is limited [12], while $\Gamma(r)$ is

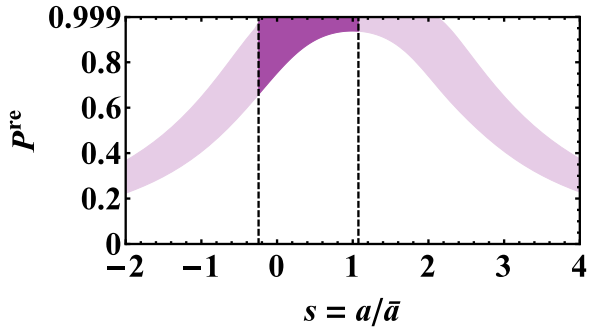

FIG. 5. Comparison between the measured PI loss rate and the MQDT prediction for nonuniversal loss [Eq. (5) including finite temperature corrections], where the purple band represents the combinations of P^{re} and s that match L_2^{PI}. The vertical dashed lines give the bounds on the scattering length from our analysis of hyperfine changing collisions, which constrains the possible combinations to the darker part of the purple band.

completely lacking. Stationary afterglow experiments at thermal energies [15] gave an anomalously large loss rate for Rb, compared to Na, K, and Cs, and from this loss rate one estimates $P^{\mathrm{re}} \approx 1$ using the classical Gorin model [29] and assuming a statistical weight of 1/3 for doublet scattering. The presence of autoionizing Rb states close to the excitation energy of He^* was suggested as a possible explanation of this anomaly [15], however, no fingerprint of these additional ionization channels was found in the electron emission spectrum [12]. *Ab initio* calculations of $V(r)$ and $\Gamma(r)$ are required to resolve this issue, however, it is probably safe to assume that $P^{\mathrm{re}} > 0.5$.

While for $a + A$ and $a + C$ PI is the only exothermic, spin-allowed two-body loss process, for $h + A$ hyperfine changing collisions (HCC) provide an additional two-body loss channel. However, comparing the loss rates for $a + C$ and $h + A$ suggests that the HCC contribution is small. By determining L_2^{PI} on the basis of $a + A$ and $a + C$ only, and obtaining a lower limit of the PI contribution for $h + A$ via $\varphi_D L_2^{\mathrm{PI}}$, we derive an upper limit of HCC loss rate of $1.2 \times 10^{-10}\ \mathrm{cm^3\ s^{-1}}$. According to the theory of ultracold spin-exchange collisions, as derived for hydrogen or alkali-metal atoms, the HCC loss rate depends on the difference between the scattering lengths of the two interaction potentials. Applying the analytical result of Ref. [30] directly to He^*+alkali collisions, with our HCC upper limit we derive that $|a_D - a_Q| < 23a_0$ (see Supplemental Material [26]). With our previously determined value $a_Q = 17(4)a_0$ [13], this would correspond to $-10a_0 < a_D < 44a_0$. This constraint significantly reduces possible values of P^{re}, as indicated by the darker part of the purple band in Fig. 5. However, this analysis assumes that there is no influence of the PI channel on the HCC process, which may be too simplistic.

In general the doublet character φ_D is magnetic field dependent, and therefore also the loss rate. For instance, for the energetically lowest spin channel $a + A$, φ_D becomes significantly less than 1/6 when $B \sim E_{\mathrm{HFS}}/4\mu_B$, and $\varphi_D \to 0$ as B^{-2} for $B \gg E_{\mathrm{HFS}}/4\mu_B$ (see Supplemental Material [26]). While for ^{87}Rb this behavior occurs at rather high magnetic fields ($E_{\mathrm{HFS}}/4\mu_B = 1.2$ kG), due to the large E_{HFS}, for an alkali-metal atom with a small E_{HFS}, like ^{41}K, this effect takes place within an experimentally accessible range of magnetic fields ($E_{\mathrm{HFS}}/4\mu_B = 45$ G). This provides interesting prospects for realizing stable ultracold mixtures in a variety of spin-state combinations, and the application of Feshbach resonances to tune the scattering length, which requires small two-body losses [31].

In conclusion, we have realized an ultracold, optically trapped mixture of $^4He^*$ and ^{87}Rb atoms and obtained the two-body loss rate coefficients for four different spin mixtures. We find long trapping lifetimes for the purely quartet spin-state combination, indicating a strong suppression of Penning ionization by at least two orders of magnitude, providing good prospects of realizing dual Bose-Einstein condensates. For the other spin mixtures we observe short lifetimes that depend on the doublet character, which suggests suppression of Penning ionization at higher magnetic fields, experimentally feasible for alkali-metal atoms with a small hyperfine splitting. We have compared our measured loss rates with recent predictions of MQDT for reactive collisions involving a strong exothermic loss channel. We observe near-universal loss for the doublet potential, and obtain a constraint on the unknown doublet scattering length.

Ultracold collisions between He^* and alkali-metal atoms can exhibit magnetically induced Feshbach resonances [32] due to the hyperfine coupling between the doublet $^2\Sigma^+$ and quartet $^4\Sigma^+$ potentials. In combination with PI these atomic collision systems provide a relatively simple and experimentally feasible platform to study the effect of a strong exothermic loss channel on Feshbach resonances [31,33], which may be important for evaporative and sympathetic cooling for molecules. Our analysis of the Penning-ionization loss rate assumes no coupling between the doublet and quartet interaction potentials, which is corroborated by the observed linear dependence of the doublet character. However, around interspecies Feshbach resonances we expect a breakdown of this simple scaling, which opens the possibility of Feshbach spectroscopy despite strong two-body losses. More elaborate MQDT calculations [34] or numerical coupled-channel calculations using *ab initio* potentials are needed to investigate the behavior of the Penning-ionization loss rate around these Feshbach resonances.

We acknowledge Rob Kortekaas for excellent technical support. We thank Piotr Żuchowski, Hartmut Hotop, Paul Julienne, Bo Gao, and Krzystof Jachymski for fruitful discussions. This work was financially supported by the Netherlands Organization for Scientific Research (NWO) via VIDI Grant No. 680-47-511 and the Foundation for Fundamental Research on Matter (FOM) via Projectruimte Grant No. 11PR2905.

[1] P. S. Julienne and F. H. Mies, J. Opt. Soc. Am. B **6**, 2257 (1989).
[2] G. Quéméner and P. S. Julienne, Chem. Rev. **112**, 4949 (2012).
[3] T. Kraemer, M. Mark, P. Waldburger, J. G. Danzl, C. Chin, B. Engeser, A. D. Lange, K. Pilch, A. Jaakkola, H.-C. Nägerl, and R. Grimm, Nature (London) **440**, 315 (2006).
[4] S. Knoop, F. Ferlaino, M. Mark, M. Berninger, H. Schöbel, H.-C. Nägerl, and R. Grimm, Nat. Phys. **5**, 227 (2009).
[5] S. Ospelkaus, K.-K. Ni, D. Wang, M. H. G. de Miranda, B. Neyenhuis, G. Quéméner, P. S. Julienne, J. L. Bohn, D. S. Jin, and J. Ye, Science **327**, 853 (2010).
[6] S. Knoop, F. Ferlaino, M. Berninger, M. Mark, H.-C. Nägerl, R. Grimm, J. P. D'Incao, and B. D. Esry, Phys. Rev. Lett. **104**, 053201 (2010).
[7] R. V. Krems, Phys. Chem. Chem. Phys. **10**, 4079 (2008).
[8] Z. Idziaszek and P. S. Julienne, Phys. Rev. Lett. **104**, 113202 (2010).
[9] B. Gao, Phys. Rev. Lett. **105**, 263203 (2010).
[10] K. Jachymski, M. Krych, P. S. Julienne, and Z. Idziaszek, Phys. Rev. Lett. **110**, 213202 (2013).
[11] A. B. Henson, S. Gersten, Y. Shagam, J. Narevicius, and E. Narevicius, Science **338**, 234 (2012).
[12] M.-W. Ruf, A. J. Yencha, and H. Hotop, Z. Phys. D **5**, 9 (1987).
[13] S. Knoop, P. S. Żuchowski, D. Kędziera, Ł. Mentel, M. Puchalski, H. P. Mishra, A. S. Flores, and W. Vassen, Phys. Rev. A **90**, 022709 (2014).

[14] H. L. Hickling, L. A. Viehland, D. T. Shepherd, P. Soldán, E. P. F. Lee, and T. G. Wright, Phys. Chem. Chem. Phys. **6**, 4233 (2004).

[15] C. E. Johnson, C. A. Tipton, and H. G. Robinson, J. Phys. B: At. Mol. Phys. **11**, 927 (1978).

[16] L. J. Byron, R. G. Dall, and A. G. Truscott, Phys. Rev. A **81**, 013405 (2010).

[17] L. J. Byron, R. G. Dall, W. Rugway, and A. G. Truscott, New J. Phys. **12**, 013004 (2010).

[18] D. Kędziera, Ł. Mentel, P. S. Żuchowski, and S. Knoop, Phys. Rev. A **91**, 062711 (2015).

[19] H. P. Mishra, A. S. Flores, W. Vassen, and S. Knoop, Eur. Phys. J. D **69**, 52 (2015).

[20] A. S. Flores, H. P. Mishra, W. Vassen, and S. Knoop, Appl. Phys. B **121**, 391 (2015).

[21] The polarizability of He^* is 1.4 times larger than Rb at a wavelength of 1557 nm [35,36], while at our ODT power gravity gives a 5% reduction on the Rb trap depth (which for He^* is well below 1%). The interspecies thermalization rate is small ($0.01s^{-1}$) due to the small interspecies scattering length [13] and the large mass ratio, and only intraspecies thermalization takes place (for which the rate is about $1s^{-1}$ for both species).

[22] W. Vassen, C. Cohen-Tannoudji, M. Leduc, D. Boiron, C. Westbrook, A. Truscott, K. Baldwin, G. Birkl, P. Cancio, and M. Trippenbach, Rev. Mod. Phys. **84**, 175 (2012).

[23] J. Söding, D. Guéry-Odelin, P. Desbiolles, F. Chevy, H. Inamori, and J. Dalibard, Appl. Phys. B **69**, 257 (1999).

[24] A. Marte, T. Volz, J. Schuster, S. Dürr, G. Rempe, E. G. M. van Kempen, and B. J. Verhaar, Phys. Rev. Lett. **89**, 283202 (2002).

[25] J. S. Borbely, R. van Rooij, S. Knoop, and W. Vassen, Phys. Rev. A **85**, 022706 (2012).

[26] See Supplemental Material at http://link.aps.org/supplemental/10.1103/PhysRevA.94.050701 for further information about the (magnetic-field-dependent) doublet character, finite temperature corrections, hyperfine changing collisions, and an overview of the measured loss rate coefficients.

[27] W. H. Miller, J. Chem. Phys. **52**, 3563 (1970).

[28] J. S. Cohen, R. L. Martin, and N. F. Lane, Phys. Rev. A **31**, 152 (1985); K. F. Scheibner, J. S. Cohen, R. L. Martin, and N. F. Lane, *ibid.* **36**, 2633 (1987); A. Merz, M. Müller, M.-W. Ruf, and H. Hotop, Chem. Phys. **145**, 219 (1990); M. Movre, L. Thiel, and W. Meyer, J. Chem. Phys. **113**, 1484 (2000).

[29] K. Jachymski, M. Krych, P. S. Julienne, and Z. Idziaszek, Phys. Rev. A **90**, 042705 (2014).

[30] H. T. C. Stoof, J. M. V. A. Koelman, and B. J. Verhaar, Phys. Rev. B **38**, 4688 (1988).

[31] J. M. Hutson, New J. Phys. **9**, 152 (2007).

[32] C. Chin, R. Grimm, P. S. Julienne, and E. Tiesinga, Rev. Mod. Phys. **82**, 1225 (2010).

[33] J. M. Hutson, M. Beyene, and M. L. González-Martínez, Phys. Rev. Lett. **103**, 163201 (2009).

[34] Z. Idziaszek, A. Simoni, T. Calarco, and P. S. Julienne, New J. Phys. **13**, 083005 (2011).

[35] M. S. Safronova, B. Arora, and C. W. Clark, Phys. Rev. A **73**, 022505 (2006).

[36] R. P. M. J. W. Notermans, R. J. Rengelink, K. A. H. van Leeuwen, and W. Vassen, Phys. Rev. A **90**, 052508 (2014).